JOURNAL OF SPACECRAFT AND ROCKETS
Vol. 33, No. 1, January–February 1996

Grid Fin Aerodynamics for Missile Applications in Subsonic Flow

John E. Burkhalter* and Harris M. Frank†
Auburn University, Auburn, Alabama 36849

The aerodynamic analysis of grid fin configurations has been extended to generic cruciform configurations oriented at any azimuthal angle. The generality of grid fin designs has been retained providing orientations for up to four fins as mounted on or near the surface of a missile airframe. The theoretical analysis is based on a vortex lattice overlay of the lifting elements and includes appropriate body upwash terms as well as wing–body carryover load prediction. This basic approach produces adequate modeling for small angles of attack and small fin incidence angles for any grid fin located at any azimuthal position around the body. For higher angles of attack, empirical equations have been developed for fin coefficients and for the body aerodynamic coefficients. Entire four-fin configurations are generically modeled, and solutions are obtained in an iterative manner. Excellent agreement between experimental data and theoretical predictions has been obtained for the configuration considered up to angles of attack of 20 deg and fin incidence angles of 30 deg. For grid fin designs other than the one considered in the wind-tunnel test and for higher angles of attack, the agreement between the theory and experimental results has not yet been established.

Nomenclature

C_{Av} = axial-force coefficient for the top and bottom fins (fins 1 and 3)
C_{Ax} = fin axial-force coefficient
C_{Axf} = fin or body viscous friction drag coefficient
C_{Axp} = fin interference drag coefficient
C_{dp} = fin pressure drag coefficient
C_H = fin chord length
C_{Mmc} = moment coefficient produced by the fin about the moment center
C_{Mmcb} = moment coefficient produced by the body about the moment center
C_{Mv} = pitching-moment coefficient for the top and bottom fins (fins 1 and 3)
C_{Nb} = normal-force coefficient for the body
C_{Nf} = fin normal-force coefficient as computed from vortex lattice theory
C_{Nv} = normal-force coefficient for the top and bottom fins (fins 1 and 3)
$C_{N\alpha}$ = normal-force coefficient slope; $dC_N/d\alpha$
fr = fineness ratio
L_b = total length of the body
L_{ref} = reference length for the configuration
M = Mach number
np = number of fin element intersection points
q_∞ = freestream dynamic pressure
R_b = radius of the body (maximum)
R_t = radius of the body at the aft end
S_l = slant length of a grid fin element
S_{ref} = reference area for the configuration
S_{wetw} = fin wetted area
t = thickness of an element of a grid fin
X_{cb} = axial distance from the nose to the body neutral point
X_{hing} = axial distance from the nose to the fin hinge line
X_{mc} = axial distance from the nose to the moment center
α = angle of attack
δ = fin incidence angle

Received Nov. 16, 1994; revision received May 29, 1995; accepted for publication May 31, 1995.

*Professor, Aerospace Engineering Department. Associate Fellow AIAA.
†Research Assistant, Aerospace Engineering Department. Member AIAA.

Introduction

SINCE the introduction of the grid fin[1] in the mid 1980s, a concerted effort has been under way to understand the complex aerodynamics associated with the internal and external flowfield of the grid fin structure. A more recent study[2] pointed out the inadequacy of present linear methods in predicting grid fin aerodynamics especially at angles of attack above 5–8 deg.[2,3] The basic configuration considered by most studies has centered around a body–fin arrangement as shown in Fig. 1, which shows the general four-fin cruciform arrangement found on most missiles. The fin itself is a lattice network (see Fig. 2) of lifting elements surrounded by an external boundary that is usually thicker than individual fin elements. As pointed out in Ref. 2 and clearly demonstrated in Refs. 4–7, the attractiveness of a grid fin over a conventional fin is based on the fact that grid fins do not stall in the conventional sense and do not demonstrate a sharp break in their loading properties even at total flow angles of 45–50 deg. In addition to this docile behavior at high angles, the fin itself produces minimal hinge moments at all angles, which means that actuator requirements for missile operation are extremely low. The reason for these small hinge moments is because the chord length on most practical grid fins is very small compared with the fin height and fin semispan.

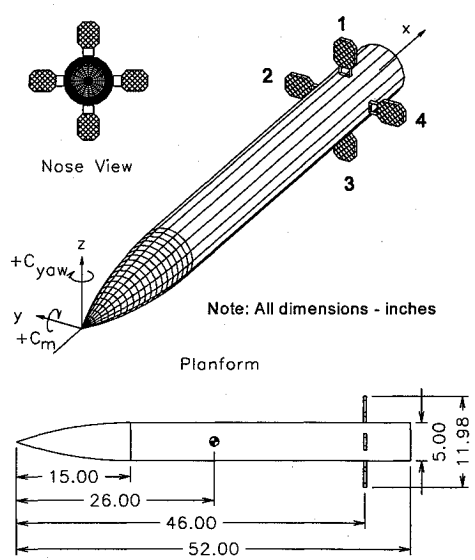

Fig. 1 Schematic of a grid fin missile configuration.

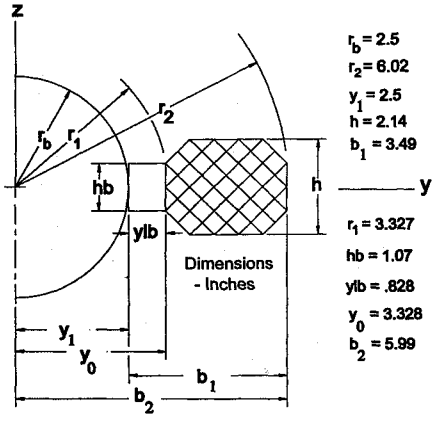

Fig. 2 Schematic of a grid fin layout on a missile body.

The present research has centered around an extension and generalization of the theoretical methodology begun in Ref. 1 to predict the aerodynamic forces and moments produced by the grid fin lifting surface as it is attached to a missile body as shown in Fig. 1. Restrictions have been made to subsonic compressible flow, but the present formulation has been generalized and extended to the four-fin case. It is clear from previous studies[1–3] that a vortex lattice formulation is the method of choice for the linear aerodynamic range, but this method must be accompanied by a well-formulated extension to higher angles for any practical use of grid fins. Experimental studies[3–6] have demonstrated the need for a nonlinear analysis and for a complete theoretical generalization to the typical missile configuration.

The empirical formulation developed for the present four-fin cruciform configuration has relied on existing wind-tunnel data[8] for the basic formulation but not to the extent that a simple curvefit was used. On the contrary, it is believed that the methodology utilized in the present analysis would also suffice for other types of lifting surfaces other than the grid fin. However, it appears that the formulation for the fin normal-force coefficient is particular well suited for grid fin applications. For body aerodynamics, an extension into the nonlinear range was also required and the basic methods as outlined in Ref. 2 were used. Modifications were made to the manner that fin–body carryover loads were implemented, making the entire process more general and generic.

Theoretical Analysis

The theoretical development for placing a system of vortices on a generic grid fin follows closely that of Refs. 2 and 3. Each grid cell is made up of a four-sided parallelogram and vortices are placed on each of these sides. An element is defined to be one of the sides of the parallelogram on which the bound portion of vortices are placed. An element is divided into a rectangular array of subelements (lattice network) and on each subelement a single bound vortex is placed along the quarter-chord of the subelement. Usually, a large number of vortices placed on each element are not required for good accuracy, and the use of a single vortex on each element will accurately predict grid fin loading for most cases.

Grid Fin Geometry and Coordinate System

The design of a grid fin for some specific missile application must follow basic geometric constraints.[2] The fin is modeled with a series of vortices, control points, and normal vectors as defined in a body-fixed coordinate system as shown in Fig. 1. The grid points that establish the intersection points of a fin are generated using the method discussed in Ref. 2. When these points are connected and given a chord depth, the three-dimensional aspects of the grid fin are established.

If one considers a single element of a grid fin located in position 2 on the body (right side looking forward as shown in Fig. 2), the element would appear as a flat plate as shown in Fig. 3. The plane of the element is defined by the three points designated as the inboard point i, the outboard point o, and one chord length in the x direction from point i. A control point p is established at the three-fourths chord point of the element, centered between the trailing legs, and a

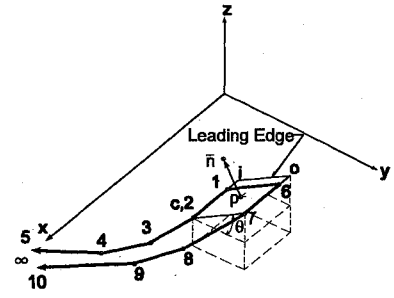

Fig. 3 Schematic of an element and coordinate system.

unit normal vector is erected at this point. From Fig. 3, the positive unit normal vector to the element may be written as

$$\bar{n}_p = (x_{p1} - x_p)\bar{i} + (y_{p1} - y_p)\bar{j} + (z_{p1} - z_p)\bar{k} \qquad (1)$$

where (x_{p1}, y_{p1}, z_{p1}) defines the coordinate location at the end of the unit normal vector.

The bound vortex is then defined on the surface of the element at the quarter-chord point. The entire horseshoe vortex was arbitrarily broken up into 10 discrete segments. The junction between each segment is defined to be a node, and the nodes that define the vortex geometry are numbered 1–10. Nodes 1 and 6 are the inboard and outboard points, respectively, of the bound portion of the vortex, whereas nodes 1–5 and nodes 6–10 establish the trailing legs of the vortex as shown in Fig. 3.

The entire geometry, including vortices, control points, and normal vectors that define each element composing each grid fin, are first generated in position 2 (see Fig. 1) on the missile body, and then all of these points are rotated through some fin incidence angle δ about the fin hinge line and then through some azimuthal angle ϕ about the body centerline to their final position on the body. Therefore, for each element there are 12 points that must be rotated through the angle δ to re-establish the orientation of the element after rotation. Points 1–10 are the vortex nodal points, point 11 is the control point, and point 12 is the unit normal endpoint. Each of the 12 points that define the element are pitched about the hinge line and rolled about the body centerline resulting in new coordinate locations defined as

$$\begin{aligned} x_p &= (x - x_{hl})\cos\delta + z\sin\delta + x_{hl} \\ y_p &= (x - x_{hl})\sin\delta\sin\phi + y\cos\phi - z\cos\delta\sin\phi \\ z_p &= -(x - x_{hl})\sin\delta\cos\phi + y\sin\phi + z\cos\delta\cos\phi \end{aligned} \qquad (2)$$

Finally, the elements and vortices that are required to generate a total of four fins are defined in this manner to create the final configuration lifting surfaces.

Vortex Lattice Solution

A vortex lattice solution was used to model the grid fin lattice network as well as the grid fin support structure. That is, vortices were placed on both the elements that make up the grid fin and the elements that make up the support structure. The entire system of elements, therefore, constituted a fin design and determined the loading carried by the grid fin. The aerodynamic fin–body carryover loads, the fin–fin interference effects, and the loading created by the missile body upwash were also included in the analysis.

Boundary conditions on the surface of a grid fin element were established by forcing the total velocity normal to an element control point to be zero. In the case of the grid fin, the total velocity at a control point is composed of three components: 1) the freestream velocity component, 2) the body-induced upwash component, and 3) the induced velocity from each of the vortex filaments in the grid fin system. The third of these components, vortex-induced velocity, can be separated into two categories: 1) the velocity induced by vortices on the same grid fin as the control point in question and 2) the velocity induced by vortices on grid fins other than that of the current control point. This division of induced velocities into two categories facilitates an iterative solution that accurately includes

fin–fin interference effects. This iterative process will be described in a later section.

For body upwash considerations, the axisymmetric body was modeled as an infinite cylinder composed of an infinite line doublet. Efforts to model the body with point sources/sinks and doublets were completed in previous studies[2,3] and were successful in computing the additional loads due to upwash. However, a comparison of the source/sink and doublet solution and the infinite line doublet solution revealed that little difference existed between the two approaches, with the exception that, for the source/sink and doublet solution, the computer run time increased. Consequently, the source/sink and doublet solution was abandoned, and an infinite line doublet was employed in all subsequent analyses. The induced velocity from the doublet and freestream can therefore be written in vector form as

$$\bar{V}_0 = \cos\alpha\bar{i} + (-V_\theta \sin\theta + V_r \cos\theta)\bar{j} + (V_\theta \cos\theta + V_r \sin\theta + \sin\alpha)\bar{k} \tag{3}$$

Therefore, the velocity component normal to an element at a control point is obtained by the dot product of the induced velocity and a unit normal to the surface at the control point. For the contribution due to vortex filaments, the Biot–Savart law, which is summarized in Ref. 2, may be used.

Iteration Procedure

Because of the usual problems in dealing with large matrices on smaller computers, it was decided that an iterative procedure would be useful in finding the vortex strengths. The solution process is as follows. First, the vortex strengths of fin 1 are found as if no other fins were present. Second, the vortex strengths of fin 2 are found as if only fins 1 and 2 exist, but the strengths of fin 1 are known, and the only unknowns are the vortex strengths of fin 2. This process continues for fins 3 and 4, each time including the known vortex strengths of the previous grid fins. When the vortex strengths of fin 4 have been found, the entire process is repeated for several iterations until the updated vortex strengths are no longer significantly different from the values of the previous iteration. In this process, inversion of large matrices is kept to a minimum, and from experience, large numbers of iterations are not required for the vortex strengths to converge. Typically, four iterations are sufficient for adequate convergence.

Linear Force Coefficients

The aerodynamic loads on a grid fin can be computed directly from the vortex strengths by considering the loading on a single element. From the Kutta–Joukowski theorem, the force coefficient C_F acting on any given element is

$$C_F = \frac{2 * \Gamma * S_l}{S_{\text{ref}}} \tag{4}$$

It follows from Eq. (4) that, in the master coordinate system, C_N is given by

$$C_N = C_F * u_{nz} \tag{5}$$

Similarly, the side-force and axial-force coefficients are given by multiplying Eq. (4) by u_{ny} and u_{nx}, respectively.

The expressions in Eqs. (4) and (5) account for that part of the fin that is exposed outside the body. The wing carryover loads were modeled by imaging the grid fin wing inside the body. It is assumed that the image element inside the body carries the same load as its companion real element outside the body. The image element may be geometrically defined by imaging each end of the outside element area along a radial line to the center of the body and then assuming that the chordwise length of the image element is the same as the exposed element chordwise length. The procedure is relatively simple and realistic carryover loads were obtained. The imaging concept is shown schematically in Fig. 4. The basic assumption for the image wing is that the normal force per unit span for the element outside the body is the same as normal force per unit span for the element inside the body. This may be expressed in coefficient form as

$$\Delta C_{Ni} = \Delta C_N (S_{ab_i}/S_{ab}) \tag{6}$$

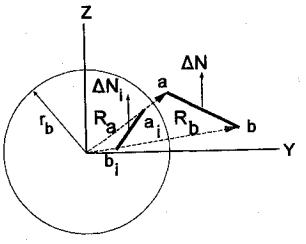

Fig. 4 Schematic of an element imaged inside the body.

where, from Fig. 4,

$$S_{ab} = \sqrt{(y_a - y_b)^2 + (z_a - z_b)^2}$$
$$S_{ab_i} = \sqrt{(y_{a_i} - y_{b_i})^2 + (z_{a_i} - z_{b_i})^2} \tag{7}$$

and

$$y_{ai} = \frac{y_a r_b^2}{R_a^2} \qquad z_{ai} = \frac{z_a r_b^2}{R_a^2}$$
$$y_{bi} = \frac{y_b r_b^2}{R_b^2} \qquad z_{bi} = \frac{z_b r_b^2}{R_b^2} \tag{8}$$

The side-force coefficient due to carryover loads is determined in a similar manner, and the axial forces were not imaged.

Finally, all forces are summed for each element and each fin to obtain the resulting linear force coefficients for the exposed lifting surfaces as well as the image surfaces. Note that because of small semispans for general grid fin applications, modeling the wing carryover loads is essential. For the designs considered in the present analysis, these loads constituted about one-third of the total.

Grid Fin Aerodynamic Coefficients and Grid Fin Normal Force

Since the vortex lattice formulation is a potential flow, inviscid solution, it is valid only in the linear angle-of-attack range that, in this case, is about 5–8 deg. Obviously, this limited angle-of-attack range is inadequate for general grid fin missile applications; consequently, existing experimental data were used to extend the range beyond the vortex lattice limit. The methods that were utilized were based on logical assumptions and basic aerodynamic principles.

The key to an empirical extension to higher angles of attack is strongly dependent on an accurate computation of the fin normal force. The form of the equation utilized in the present research is based on the observation that grid fins do not stall in the normal aerodynamic sense but continue to produce lift even at large angles of attack. The lift production does, however, peak. Therefore, the required equation must define a curve that has the traditional linear slope at $\alpha = 0$ and demonstrates a peak value at a large angle of attack $\alpha_{\max}$. From an analysis of existing wind-tunnel data,[8] the parametric equation that seems to fit the prediction of grid fin normal force is

$$C_N = \left.\frac{C_{N\delta}\delta}{1 + (\delta/\delta_{\max})^2}\right|_{\alpha=0} + \left.\frac{C_{N\alpha}\alpha}{1 + (\alpha/\alpha_{\max})^2}\right|_{\delta=0} \times \left(1 - \left.\frac{C_{N\delta}\delta}{1 + (\delta/\delta_{\max})^2}\right|_{\alpha=0}\right) \tag{9}$$

This equation is composed of three major terms and four unknowns: $C_{N\delta}$, $C_{N\alpha}$, $\delta_{\max}$, and $\alpha_{\max}$. It has the required linear limit as either δ or α approaches zero and reaches a maximum value at specified angles of attack. The mutual dependency of the fin incidence angle and the angle of attack seems to be properly modeled with the cross-coupling term.

For a grid fin, the slopes $C_{N\delta}$ and $C_{N\alpha}$ may be computed directly using the vortex lattice method outlined in a previous section. The procedure for computing these slopes is restricted to conditions in the linear range of angles of attack for both the body and fin incidence angles. If body upwash terms are neglected, $C_{N\delta}$ is computed; if body upwash terms are included, $C_{N\alpha}$ is computed.

The values of α_{max} and δ_{max} may be obtained directly from an analysis of wind-tunnel data. In each case, the angle at which the normal force reaches a maximum is noted from the data but specifically under the assumptions outlined in the theory. That is, for δ_{max}, the angle of attack must be set to 0.0, and for α_{max}, the fin incidence must be 0.0. These observations from experimental data are not very sensitive to the exact angle of α_{max} or δ_{max} but need to be as close as possible to actual maximums. The degree to which Eq. (9) agrees with the experimental data will be demonstrated in a later section. For the side-force coefficients, α_{max} and δ_{max} will be the same as for the normal-force computations.

Fins in the Vertical Position

Grid fins demonstrate a unique feature not found on any other lifting surface system currently in use on missile systems. For a fin mounted in the vertical position, fin 1 or fin 3, a normal force is still produced at any finite body angle of attack. The form of the equation to describe this normal force is still Eq. (9); however, the values of $C_{N\delta}$, and $C_{N\alpha}$ are significantly smaller than corresponding values for horizontal fins. The slopes are, however, still found with a direct application of vortex lattice theory, and the values of α_{max} or δ_{max} can still be extracted from experimental data.

An error, however, is introduced that does not show up in the linear analysis for angles as small as 5 deg used in the computations of the slopes for $C_{N\delta}$, and $C_{N\alpha}$. The error arises from the streamline flow near the top and bottom of the body surface and from the body vortices emanating from the nose. Consider the flowfield as shown schematically in Fig. 5. Without definitive data to the contrary, it is assumed that a grid fin located directly on top or bottom of the body is immersed in a stream tube that is nearly parallel to the body. The vortices on top of the body emanating from the nose also add to the complexity of the flow region at least for the top fin. In any case, it is clear that the top and bottom fins would see an oncoming flow that is not the same as the freestream direction. From an analysis of available experimental data, it is assumed that an average angle of attack for the top and bottom fin due to body alteration of the incident streamlines is about $\alpha/2$.

Fins Arbitrarily Positioned

For the general case where the fin is arbitrarily positioned on the body, the values of $C_{N\delta}$, $C_{N\alpha}$, α_{max}, and δ_{max} are dependent on the azimuthal angle at which the fins are located. The slopes $C_{N\delta}$, and $C_{N\alpha}$ may still be determined from vortex lattice theory, but the values of α_{max} for each fin make transitions from the values at the horizontal position to the values at the vertical position. It is assumed, however, that this transition for α_{max} is not a linear function of ϕ but is highly nonlinear. As an aid to understanding this nonlinearity, the assumed streamline analysis pictured schematically in Fig. 5 can be used to develop a parametric equation for defining how α_{max} changes with ϕ. If a fin is positioned slightly off the vertical position, say at an azimuthal angle of 80 deg, then the fin would see nearly the same angle of attack as the fin in the horizontal position where $\phi = 0.0$. This, of course, would depend on the diameter of the body relative to the width of the fin and perhaps on other factors. In any case, for the present analysis, it is assumed that this dependency on the azimuthal angle for α_{max} is

$$\alpha_{max} = \alpha_{max-horizontal}\left[\xi + (1-\xi)\left|\sqrt{\sqrt{\sqrt{\cos\phi}}}\right|\right]$$

$$\text{where } \xi = \frac{\alpha_{max-vertical}}{\alpha_{max-horizontal}} \tag{10}$$

The value of δ_{max} is not affected by the body since it is determined only for $\alpha = 0.0$.

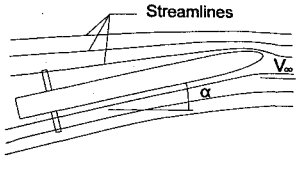

Fig. 5 Schematic of an assumed streamline flow.

A grid fin produces a pitching moment about the missile moment center that may be computed directly from the nonlinear normal-force coefficient. It is assumed that the aerodynamic center of a grid fin is near the quarter-chord, and the moment about the fin aerodynamic center is extremely small in comparison with the moment about the missile moment center. Consequently, the pitching-moment coefficient for an individual grid fin about the configuration moment center can be written as

$$C_{Mmc} = \frac{C_N(X_{mc} - X_{cp})}{L_{ref}} \tag{11}$$

The axial force on the fin (drag at $\alpha = 0.0$ deg) is assumed to be composed of induced drag, skin friction, pressure drag, and an interference drag due to fin element intersections. For the skin-friction drag, and fin wetted area is computed and converted to an equivalent flat plate area with an assumed laminar and/or turbulent boundary layer. The skin-friction coefficient, as a function of Reynolds number, is determined and finally a friction axial-force coefficient is computed as C_{Axf}. These computations for viscous axial force follow closely those in Ref. 9.

It is assumed that the pressure drag may be written as a product of the dynamic pressure and the frontal area resulting in coefficient form as

$$C_{dp} = \frac{S_{wetw}t}{2 * S_{ref}C_H} \tag{12}$$

The grid intersection points create a drag that is empirically determined from experimental data[8] as

$$C_{Axp} = 2.0 * 0.000547 * (np + 2) \tag{13}$$

where $(np + 2)$ is the total number of grid intersection points including points on the base support structure.

The nonlinear induced axial force is that contribution due to fin deflection alone and is the component of the fin force vector due to fin incidence that is in the axial direction (parallel to the body). Consequently,

$$C_{Ai} = C_N|_{\alpha=0} \tan\delta \tag{14}$$

The axial-force coefficient for the fin is then the sum of these four components:

$$C_{Ax} = C_{Axf} + C_{Axp} + C_{dp} + C_{Ai} \tag{15}$$

From experimental grid fin data, the fin axial-force coefficient changes very little over a large range of angles of attack[5,6]; consequently, it was assumed that the axial force is independent of angle of attack and is therefore constant at the value determined in Eq. (15) for some given value of fin incidence angle.

Body Aerodynamic Coefficients

The body alone aerodynamic coefficients are based on a combination of Jorgensen's theory[10] and a modified form of slender body theory. Jorgensen's theory has been shown to yield good agreement with experimental results at least for angles of attack between 30 and 60 deg. For lower angles of attack between 0 and 30 deg, the theory does not agree quite as well; consequently, a modified form of slender body theory was used.

To utilize this modified slender body theory in conjunction with Jorgensen's theory, it was required that the normal-force coefficient from each theory coincides at some specified angle of attack α_0. In the present method for body angles of attack below α_0, it is assumed that the modified slender body normal-force coefficient may be written as

$$C_{Nb} = \frac{2K_b\alpha}{K_b - \sin(2\alpha)} \tag{16}$$

where the constant K_b is determined by forcing agreement with Jorgensen's theory at α_0.

Jorgensen's method[10] may also be used to compute the body alone pitching moment. However, the pitching moment predicted by Jorgensen's method does not agree with experimental data as well as desired, especially at angles of attack below α_0. Consequently,

extensive sets of experimental data[8] from several body alone wind-tunnel tests were used to develop an equation that identifies the body alone center of pressure from which the body pitching moment could be determined. The empirical equation for the body alone neutral point resulting from this study was determined to be

$$X_{cb} = \frac{L_b}{2}\left[1 - \frac{1}{2\zeta}\right], \quad \text{where} \quad \zeta = \left[1 + \left(\frac{L_b}{2R_b}\right)\alpha^2\right] \tag{17}$$

so that the pitching-moment coefficient for the body about the moment center is

$$C_{Mmcb} = C_{Nb}\left[\frac{X_{mc} - X_{cb}}{L_{\text{ref}}}\right] \tag{18}$$

Equation (18) is used for determining the body pitching moment for angles of attack below α_0, and Jorgensen's equation may be used for angles above this value, even though in the present study the body angle-of-attack range is limited to 20 deg.

The axial force for the body at small angles of attack is assumed to be composed of the skin friction and the body base drag. From an analysis of experimental body alone wind-tunnel data, it is assumed that the body axial force is independent of angle of attack and therefore is assumed to be constant for any given configuration, Mach number, and flight condition. It will be shown later that this assumption of constant body axial force is well justified.

Results and Comparison with Experimental Data

Using the model shown in Figs. 1 and 2, the theoretical analysis was compared with data from Ref. 8. The entire test model consisted of four fins that were mounted horizontally and vertically in a cruciform configuration. Fins 2 and 4 were mounted in the horizontal as shown in Fig. 1, and fins 1 and 3 were mounted in the vertical on top and bottom of the missile airframe. Data were collected for configurations that included 1) the body alone, 2) the body plus two horizontal fins, and 3) the entire four-fin–body arrangement. For some of the tests, fins 2 and 4 were mounted on individual fin balances and were rotatable to discrete incidence angles, whereas fins 1 and 3 were fixed and rigidly attached to the body. Comparisons between the experimental data and the theoretical computations were made for several configuration combinations. In all experimental test data, the Mach number was maintained at $M = 0.5$, and the Reynolds number, based on the body diameter, was held constant at 22.7×10^6. For these tests, the standard body-fixed sign convention was used as shown in Fig. 1. All linear dimensions were nondimensionalized by the span of a single grid fin (see Fig. 2) that is analogous to the wing semispan on normal wing–body combinations. The reference length was the maximum body diameter, and the reference area was the maximum body cross-sectional area.

Body Alone

Figure 6 is a plot of the body alone normal-force, pitching-moment, and axial-force coefficients. Agreement up to 20 deg angle of attack is acceptable for this case for normal force and pitching moment, but the predicted axial force is about 30% low as shown in Fig. 6. It is believed that the major error in the axial-force coefficient is in the base drag approximations, and additional analyses are needed to correct this deficiency.

Fin Alone

Figure 7 is a plot of the fin 2 normal-force coefficient showing a comparison of the theory using Eq. (9) with experimental data at a fin incidence angle of 0 deg. This figure was generated from an analysis of a single fin alone and does not include the wing–body carryover loads. The several lines of experimental data in this figure resulted from extracting fin 2 normal-force coefficients from several sets of experimental data. Some of the data were obtained directly from fin balances and some were extracted from the main body balance. By comparing these data with four-fin data to be presented later, it was determined that for the grid fin a significant part of the load can be carried by the body as a wing carryover load.

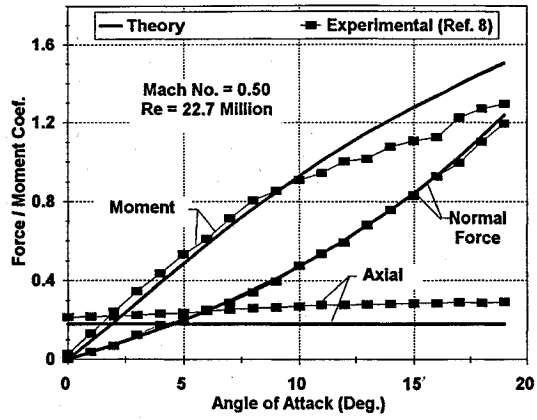

Fig. 6 Body alone normal-force, axial-force, and pitching-moment coefficients.

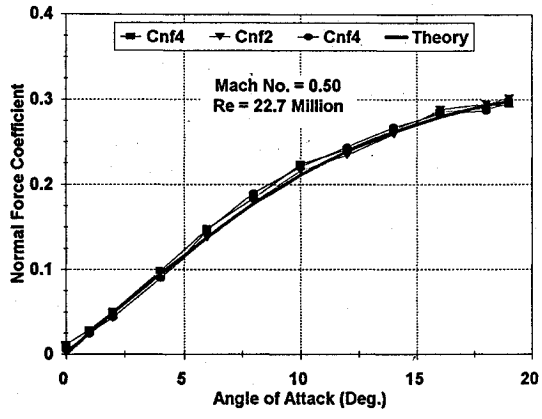

Fig. 7 Fin-alone normal-force coefficient for a fin deflection of 0 deg.

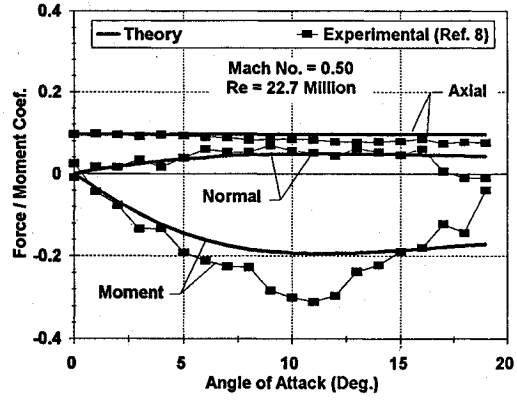

Fig. 8 Normal-force, axial-force, and pitching moment coefficients for vertical fins 1 and 3 for a fin deflection of 0 deg.

Even though the data are not plotted, comparisons were made for the normal-force coefficients of fin 2 at various azimuthal angles around the body using Eqs. (9) and (10). These comparisons showed that the normal-force coefficient decreases from a value of about 0.40 in the unrolled case to about 0.025 in the top 90-deg rolled case. However, for four fins in a cruciform arrangement, the total normal force does not vary significantly for roll angles above about 3 deg. That is, if there are four fins 90 deg apart, and the entire configuration is rolled about the body centerline, the total normal force remains essentially constant. The exception of this general trend occurs when the missile is in the cruciform nonrolled configuration, in which case the top and bottom fins have a lower normal force due to the streamline flow, as pictured in Fig. 5.

Fin Loading with Body Upwash and Wing–Body Carryover Loads

Figure 8 is a comparison of normal force, pitching moment, and axial force for the top and bottom fin, 1 and 3. Fins 1 and 3 are rigidly attached to the body and develop less lift and pitching moment

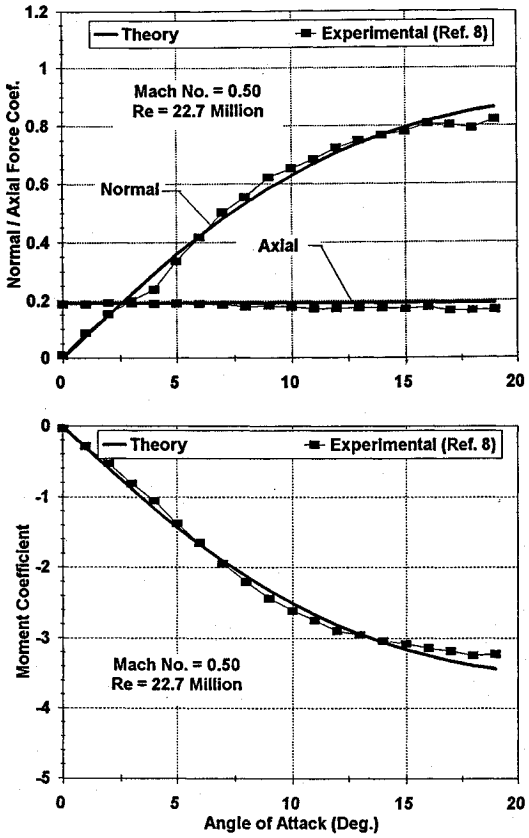

Fig. 9 Normal-force, axial-force, and pitching-moment coefficients for a fin deflection of 0 deg.

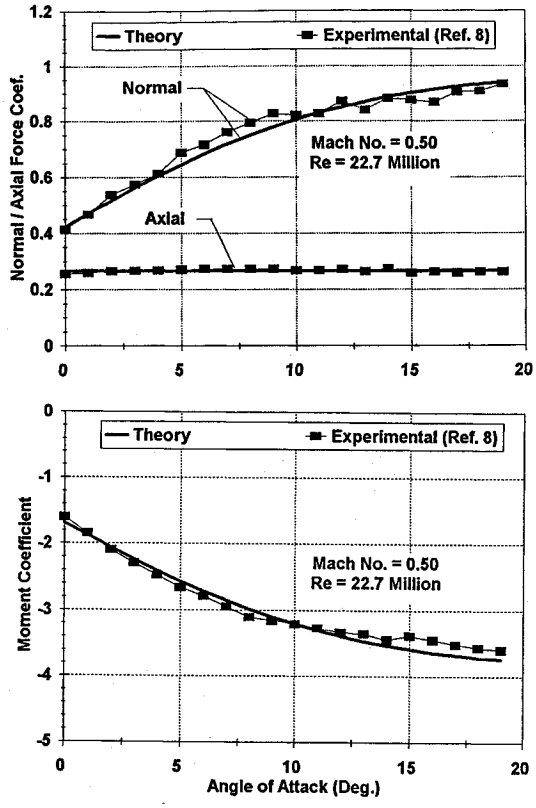

Fig. 10 Normal-force, axial-force, and pitching-moment coefficients for a fin deflection of 10 deg.

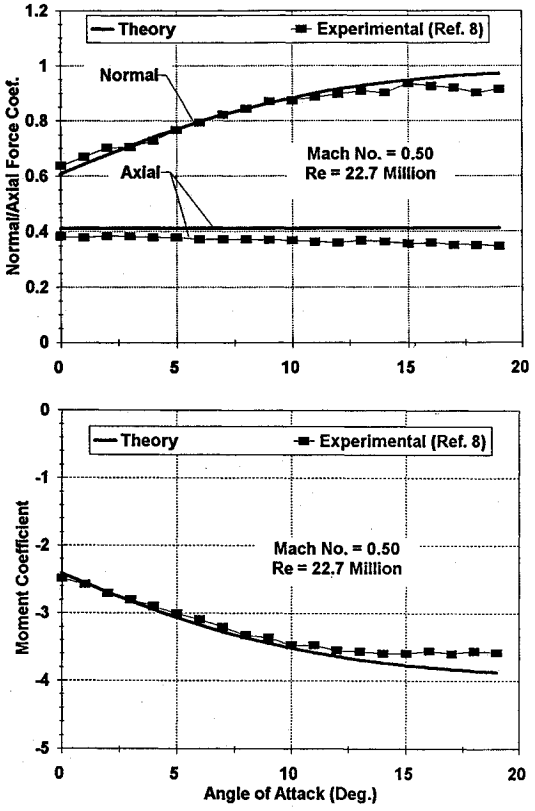

Fig. 11 Normal-force, axial-force, and pitching-moment coefficients for a fin deflection of 20 deg.

than fins 2 and 4, especially at higher angles of attack. The significant scatter in the experiment is attributed to the turbulent, vortex-dominated flowfield on top of the body and to the inaccuracies in the main balance load cell for small normal forces generated by the vertical fins. Figure 9 is a comparison of the normal force, axial force, and pitching moment for a four-fin combination that includes the wing–body carryover loads. Agreement between the theoretical and experimental data is good and is well within the experimental accuracy of the balance. The discrepancy at higher angles of attack is directly attributed to the overprediction of the normal force of fins 1 and 3.

Figures 10–12 are four-fin comparison plots for horizontal fin incidence angles of 10, 20, and 30 deg, respectively. It is clear that, for most of these cases, the agreement is good but appears to break down at total fin angles above 40–45 deg. It is apparent from Figs. 11 and 12, that grid fins do not actually stall in the classical aerodynamic sense; however, somewhere between a fin total angle of attack of 30 and 50 deg, the normal force peaks, which is followed by a significant dropoff but not a stall in the classical sense, even at 50 deg.

The agreement between the experimental data and the theory is remarkable, given the large fin angles (up to a total of 50 deg for the 30-deg incidence case). It also seems that at high incidence angles the assumption of constant axial-force coefficient over the range of angles of attack is a valid assumption, but the methods used to compute the magnitude of the fin axial forces are somewhat in error. Figure 13 is a plot of the theoretical four-fin axial force over the incidence angle range of 0–45 deg. The theory agrees with experiment up to (and beyond) 10-deg incidence; however, at higher angles, the theoretical predictions break down and further work should be done in this area to more accurately model the magnitude of the fin axial-force coefficient due to fin incidence alone.

Experimental Accuracy

The balances used in the experimental wind-tunnel test included two fin balances attached to fins 2 and 4 and a main balance with its electrical center at the moment center of the model (see Fig. 1). The quoted accuracy of the fin balances is 2.5% of the rated loads, which, in this case, results in an accuracy of ±5 lb for the normal force and ±5 in.-lb for the pitching moment. The main balance is quoted to be 0.25% of the rated loads or ±7 lb for the normal force, ±11 in.-lb for the pitching moment, and ±1 lb for the axial force. Even though the balance accuracy is quoted to have large uncertainties, the repeatability proved to be much better. In each case, the repeatability for each balance was quoted to be within 0.1% of rated loads.

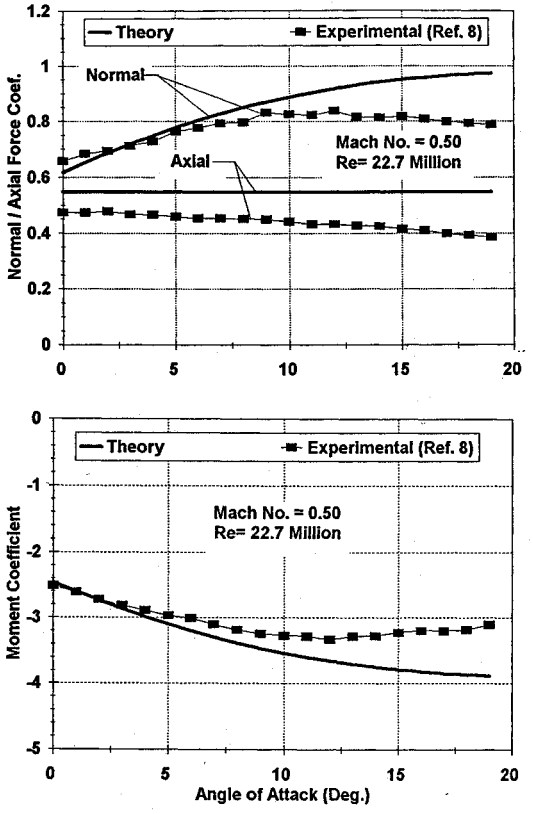

Fig. 12 Normal-force, axial-force, and pitching-moment coefficients for a fin deflection of 30 deg.

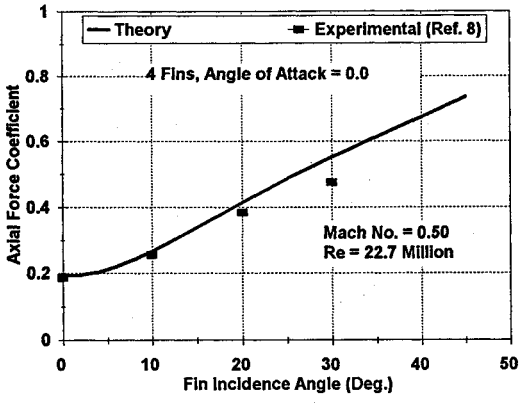

Fig. 13 Fin axial-force coefficients vs fin incidence angle.

Conclusions

As a result of the mathematical modeling and the analysis of the available experimental data, the following conclusions are made.

1) The theoretical methods developed for modeling the aerodynamics of grid fins appear to be adequate for design purposes. The empirical equations provide good agreement with experimental data over a wide range of angles of attack, validating, to some extent, the assumptions made at the outset. Vortex lattice theory has been proven to be adequate for the basic linear range of load and moment coefficient prediction and the initial slopes are accurately predicted provided the carryover loads are included as well as the upwash effects from the body.

2) Although the agreement with experimental data appears to be very good up to about 45 deg total angle of attack, extension beyond this range is uncertain. The extensions of the theory to include nonlinear effects appear to be in the right direction but have not been verified for grid fin shapes other than the one considered in the present work.

3) The proper relationship between the loads and moments due to fin incidence and fin–body angle of attack has been properly modeled at least for angles below 45 deg total angle of attack.

4) Modeling of the body forces and moments is adequate up to about 20 deg but, for the present configuration, has not been validated for higher angles using Jorgensen's method.

5) Some of the uncertainty in the analysis appears to be associated with the internal flowfield inside a grid fin. Experimental data to describe the flowfield details internal to the grid elements are lacking, and one cannot be certain as to the effects that mutual wall interference flows will have on the overall loading especially at higher angles of attack. Because of the uncertainty at these angles, additional research into the details of the internal flowfield must be done before further empiricism is utilized in predicting the fin loads and moments for higher angles of attack.

References

[1]Belotserkovskiy, S. M., Odnovol, L. A., Safin, Y. Z., Tyulenev, A. N., Frolov, V. P., and Shitov, V. A., "Wings with Internal Framework," Machine Translation, FTD-ID(RS)T-1289-86, Foreign Technology Div., Wright–Patterson AFB, OH, Feb. 1987.

[2]Burkhalter, J. E., Hartfield, R. J., and Leleux, T. M., "Nonlinear Aerodynamic Analysis of Grid-Fin Configurations," *Journal of Aircraft*, Vol. 32, No. 3, 1995, pp. 547–554.

[3]Brooks, R. A., and Burkhalter, J. E., "Experimental and Analytical Analysis of Grid-Fin Configurations," *Journal of Aircraft*, Vol. 26, No. 9, 1989, pp. 885–887.

[4]Washington, W. D., and Miller, M. S., "Grid-Fins—A New Concept for Missile Stability and Control," AIAA Paper 93-0035, Jan. 1993.

[5]Washington, W. D., Booth, P. F., and Miller, M. S., "Curvature and Leading Edge Sweep Back Effects on Grid-Fin Aerodynamic Characteristics," AIAA Paper 93-3480, Aug. 1993.

[6]Booth, P. F., and Washington, W. D., "Post Test Report for a Grid-Fin Technology Wind-Tunnel Test," Missile Command, U.S. Army, Rept. TR-RD-SS-89-6, Redstone Arsenal, AL, July 1989.

[7]Washington, W. D., and Booth, P. F., "Wind-Tunnel Data Analysis for a Curved Grid-Fin Concept," TTCP Technical Panel W-2, Internal Rept., Eglin AFB, FL, May 1990.

[8]Auman, L., "Aerodynamic Database User's Guide," Missile Command, U.S. Army, Rept. TR-RD-SS-92-7, Redstone Arsenal, AL, Aug. 1992.

[9]Roskam, J., *Methods for Estimating Drag Polars for Subsonic Airplanes*, published by the author, 519 Boulder St., Lawrence, KS, 1971.

[10]Jorgensen, L. H., "Prediction of Static Aerodynamic Characteristics for Slender Bodies Alone and with Lifting Surfaces to Very High Angles of Attack," NASA TM X-73, 123, July 1976.

Jerry Allen
Associate Editor